# Influence of Crystal Packing on Molecular Geometry: A Crystallographic and Theoretical Investigation of Selected Diorganotin Systems

**Mark A. Buntine, Veronica J. Hall, Frances J. Kosovel, and Edward R. T. Tiekink***

*Department of Chemistry, The University of Adelaide, Adelaide SA 5005, Australia*

*Received: September 3, 1997; In Final Form: December 4, 1997*

A combined crystallographic and theoretical study into the influence of crystal packing on molecular geometry in certain diorganotin compounds is reported. Geometry optimizations of crystallographically determined molecular geometries revealed that in the absence of crystal packing effects the molecules become more symmetric, and hence it is suggested that crystal packing can influence molecular geometry. Generally, while bond angles subtended at tin did not change significantly beyond that required to effect the symmetrization of the structure, Sn−ligand separations tended to elongate in the gas phase.

## 1. Introduction

In a number of recent surveys of the structural chemistry of main-group element compounds it has been noted that quite significant changes in the immediate environment of the central element may be found for compounds with similar chemical formulas.[1] For example, in the mercury(II) bisxanthates, $Hg(S_2COR)_2$, extraordinary changes in their solid-state structures are evident as the nature of $R$ is changed. Thus, the simple substitution of a Me for a $^n$Pr and then for an $^i$Pr results in the formation of one-, two-, and three-dimensional structures, respectively. For $R$ = Me, a linear polymeric structure is found featuring three-coordinate mercury centers.[2] Substituting the methyl for an *n*-propyl group results in the formation of sixteen-membered $[-HgSC(O^nPr)S-]_4$ rings that are interconnected laterally via additional bridging ligands to form a layer structure with tetrahedrally coordinated mercury centers.[3] A further major change in structure is evident when $R = {}^i$Pr.[4] The 16-membered rings of the $R = {}^n$Pr structure are still evident as are the tetrahedrally coordinated mercury centers. The difference arises in the connectivities between the rings which, for two of the mercury centers, now occur above and below the plane of the ring leading to a network structure; the coordination geometry about each of the two remaining mercury atoms is completed by a chelating ligand. Similar variations in structure are observed in the related dithiocarbamate ($^-S_2CNR_2$), dithiophosphate ($^-S_2PR_2$), etc., systems for which a total of eight distinct motifs have been described.[1f] Other remarkable changes in coordination patterns are evident in related main-group element systems including organotin structures,[1d,e] the focus of the present study. Here, we report on our investigations into crystal packing effects on organotin molecular geometry, using a combination of crystallographic analysis and theoretical modeling.

Organotins have many applications[5] in diverse fields such as catalysis, agrochemicals, and as potential antitumor agents. Underpinning the understanding of organotin chemical behavior is a knowledge of their molecular structure. The reason(s) for the adoption of diverse motifs in the solid state for many organotin systems are not known; however, electronic and steric factors of the organotin entities and/or ligands may play significant roles. Less tangible is the influence of crystal packing on molecular structure. While it is well-known that in the crystalline state intermolecular forces, such as dipole/dipole interactions (including hydrogen bonding), may influence the conformation for a particular residue, less well understood is the role of weaker intermolecular forces on molecular geometry. The aim of the present study is to compare geometric parameters derived from crystallographically determined structures with those calculated from ab initio geometry optimizations for a number of organotin systems in order to investigate the influence of crystal packing on molecular structure.

The availability of powerful computing resources now enable calculations to be performed on once intractable metal-containing systems. For example, ab initio calculations have been employed recently to examine the nature of metal cation interactions with nucleobases,[6] gold species with thionucleobases,[7] zinc dithiophosphates,[8] and bonding in transition-metal systems.[9] Thus, while the influence of crystal packing on conformation has been investigated for organic systems,[10] in particular with reference to polymorphism and crystal engineering through supramolecular associations, analogous studies involving the heavier elements is an emerging field.

The calculations reported here have been performed at the HF/LanL2DZ level of theory. This approach incorporates the use of the effective core potential (ECP)[11] approximation in the treatment of the tin atoms. The Hartree−Fock (HF) theoretical approach makes no account of electron correlation in the reported geometry optimizations.

Cotton and Feng[12] have undertaken a density functional theory (DFT) study focusing on geometry optimizations of a variety of transition-metal-containing dinuclear compounds. The DFT approach includes some account of electron correlation. Cotton and Feng have shown that the ECP approximation within the DFT calculations predicts molecular geometries in good agreement with both experiment and theory, where the more conventional double-$\zeta$ all-electron basis sets are commonly employed. Maduara et al.[13] have reported all-electron DFT calculations that make structural predictions of Rh-containing species that are in good agreement with X-ray diffraction data.

The previous studies cited give us confidence that the ECP approximation is a valid approach for reporting molecular geometries of transition-metal-containing species. It needs,

* Corresponding author. FAX: 61 8 8303 4358. Email: etiekink@chemistry.adelaide.edu.au.

S1089-5639(97)02872-7 CCC: $15.00 
Published on Web 03/17/1998

**TABLE 1: Crystallographic Data**

| | **2** | **3** | **4** | **5** |
|---|---|---|---|---|
| formula | $C_{21}H_{40}ClNS_2Sn$ | $C_{17}H_{17}Cl_2N_2Sn$ | $C_{17.25}H_{16.25}Cl_{2.75}N_2Sn$ | $C_{14}H_{14}Cl_2N_2Sn$ |
| formula weight | 524.8 | 438.9 | 467.8 | 399.9 |
| crystal system | triclinic | triclinic | monoclinic | orthorhombic |
| space group | $P\bar{1}$ | $P\bar{1}$ | $P2_1/n$ | *Cmcm* |
| *a*, Å | 12.761(3) | 9.260(1) | 14.039(3) | 11.321(2) |
| *b*, Å | 18.329(6) | 13.253(3) | 16.525(2) | 18.889(1) |
| *c*, Å | 12.191(3) | 7.8702(8) | 17.174(1) | 7.537(1) |
| α, deg | 97.73(3) | 95.21(1) | | |
| *β*, deg | 98.85(2) | 90.792(9) | 91.34(1) | |
| *γ*, deg | 107.90(2) | 69.76(1) | | |
| *V*, Å$^3$ | 2630(1) | 902.3(3) | 3983(1) | 1611.6(3) |
| *Z* | 4 | 2 | 8 | 4 |
| $D_{calcd}$, g cm$^{-3}$ | 1.325 | 1.615 | 1.560 | 1.648 |
| radiation, Å | Cu, 1.5418 | Mo, 0.7107 | Mo, 0.7107 | Cu, 1.5418 |
| $\mu$, cm$^{-1}$ | 101.79 | 17.09 | 16.50 | 155.80 |
| trans coeff | 0.798−1 | 0.974−1 | 0.978−1 | 0.843−1 |
| 2$\theta$ range, deg | 3.0−120.0 | 3.0−55.0 | 3.0−55.0 | 3.0−120.0 |
| no. of reflns meas | 8247 | 4413 | 9889 | 3280 |
| no. of unique reflns | 7838 | 4157 | 9516 | 3280 |
| no. of reflns used[a] | 5293 | 3261 | 5888 | 1391 |
| no. of variables | 469 | 199 | 413 | 59 |
| *R* | 0.059 | 0.029 | 0.048 | 0.046 |
| $R_w$ | 0.062 | 0.030 | 0.051 | 0.057 |
| residual e$^-$/Å$^3$ | 1.12 | 0.41 | 1.84 | 0.56 |

[a] $I \geq 3.0\sigma(I)$.

however, to be ascertained that the lack of electron correlation in our treatment does not cast some doubt on the validity of the geometric results reported here. To this end we have performed a series of calculations to compare predicted geometries for two simpler Sn-containing compounds, [$MeSnCl_3$] and [$Me_3SnCl$], using both HF and DFT levels of theory. The results of the comparative study are reported in section 3 and show that there is very good agreement in the geometric predictions generated by each theoretical approach. We are therefore satisfied that there is no need to include electron correlation in predictions of molecular geometry for metal-containing compounds, particularly Sn-containing compounds.

The diorganotin systems chosen for the focus of this study encompass a range of crystallographic circumstances. The first system to be investigated crystallizes as two polymorphs, indicating different packing arrangements. Geometry optimizations have also been performed for examples where (i) two molecules comprise the crystallographic asymmetric unit, (ii) a molecule has cocrystallized solvent, (iii) a solvate has two molecules in the asymmetric unit, and finally (iv) a structure has high symmetry (i.e., *m*2*m*). The comparison of the crystallographically determined structures with those calculated employing ab initio geometry optimizations will enable an examination of the influence that solid-state effects have on molecular geometry.

## 2. Experimental Section

**2.1. Computational Details.** All geometry optimizations were performed using the GAUSSIAN 94 suite of programs[14] run on Silicon Graphics Indigo$^2$xZ Workstation and Silicon Graphics Power Challenge computers. All calculations were performed at the Hartree−Fock SCF level of theory using the LanL2DZ basis set.[14] The LanL2DZ basis set employs the Dunning/Huzinaga double-$\zeta$ descriptor[15] for all first-row elements and replaces the core electrons of sulfur (up to 2p), chlorine (up to 2p), and tin (up to 4p) with the effective core potentials (ECPs) of Hay and Wadt.[11]

**2.2. Crystallography.** Details specific to each determination are given below, and crystallographic data are given in Table 1. Generally, intensity data were collected at room temperature on a Rigaku AFC6R diffractometer employing the $\omega$:2$\theta$ scan technique. Either graphite monochromatized Mo Kα radiation ($\lambda$ 0.710 73 Å) or Ni-filtered Cu Kα radiation ($\lambda$ 1.5418 Å) was used such that $\theta_{max}$ was 27.5 or 60.0°, respectively. The data sets were corrected routinely for Lorentz and polarization effects,[16] and an empirical absorption correction[17] was applied in each case. The structures were solved by direct methods[18−20] and each refined by a full-matrix least-squares procedure based on *F*.[16] Non-hydrogen atoms were refined with anisotropic displacement parameters and hydrogen atoms included in the models at their calculated positions (C−H 0.97 Å). A $\sigma$ weighting scheme was applied, i.e., $w = 1/\sigma^2(F)$, and the refinement continued until convergence in each case. Neutral scattering factors employed were as included in teXsan[16] and diagrams were drawn with ORTEP[21] at the 35% probability level.

**[$^t$Bu$_2$Sn(S$_2$CNcHex$_2$)Cl] (2).** The compound was prepared from the reaction of [$^t$Bu$_2$SnCl$_2$] (Aldrich) and 1 mol equiv of $KS_2CNcHex_2$ in solution following a literature procedure.[22] Crystals were obtained from the slow evaporation of an ethanol solution of the compound; mp 172−173 °C. Two molecules of the compound comprise the asymmetric unit, labeled *a* and *b*. Owing to the decrease in the net intensity values for a set of three standard reflections (approximately 11%), a correction was made to the data set assuming a linear decay. High thermal motion was noted for some of the methyl groups, however, no evidence was found for split sites.

**[Vin$_2$SnCl$_2$(bipy)]·0.5C$_6$H$_6$ (3).** The compound was isolated from a solution containing [vin$_2$SnCl$_2$] (Aldrich) and 2,2′-bipyridyl as a white powder; colorless crystals, as a hemibenzene solvate, were obtained from the slow evaporation of an acetonitrile/benzene (9/1) solution of the compound; mp 202−203 °C.

**[Me(Ph)SnCl$_2$(bipy)]·0.25CHCl$_3$ (4).** Colorless crystals were obtained from the slow evaporation of an acetonitrile/chloroform (9/1) solution of the adduct which was prepared as for **3** using [Me(Ph)SnCl$_2$] (supplied by K. Jurkschat, Dortmund); mp 253−254 °C. The asymmetric unit comprises two

**TABLE 2: Selected Geometric Parameters (Å, deg) for [$MeSnCl_3$] Obtained from X-ray, Electron Diffraction, and the LanL2DZ Basis Set at the HF, HF/DFT(B3LYP), and DFT(BLYP) Levels of Theory**

| parameter | X-ray[23] | electron diffraction[25] | HF | HF/DFT (B3LYP) | DFT (BLYP) |
|---|---|---|---|---|---|
| Sn−C | 2.074(8) | 2.10(2) | 2.098 | 2.110 | 2.128 |
| Sn−Cl(1) | 2.283(2) | 2.304(3) | 2.358 | 2.388 | 2.411 |
| Sn−Cl(2) | 2.318(1) | 2.304(3) | 2.358 | 2.388 | 2.411 |
| Sn−Cl(3) | 2.318(1) | 2.304(3) | 2.358 | 2.388 | 2.411 |
| C(1)−Sn−Cl(1) | 120.3(3) | 113.9(7) | 111.8 | 111.2 | 111.0 |
| C(1)−Sn−Cl(2) | 113.5(1) | 113.9(7) | 111.8 | 111.2 | 111.1 |
| C(1)−Sn−Cl(3) | 113.5(1) | 113.9(7) | 111.8 | 111.2 | 111.0 |
| Cl(1)−Sn−Cl(2) | 103.58(6) | 104.7(4) | 107.1 | 107.7 | 107.9 |
| Cl(1)−Sn−Cl(3) | 103.58(6) | 104.7(4) | 107.1 | 107.7 | 107.9 |
| Cl(2)−Sn−Cl(3) | 99.78(6) | 104.7(4) | 107.1 | 107.7 | 107.9 |

**TABLE 3: Selected Geometric Parameters (Å, deg) for [$Me_3SnCl$] Obtained from X-ray, Electron Diffraction, and the LanL2DZ Basis Set at the HF, HF/DFT(B3LYP), and DFT(BLYP) Levels of Theory**

| parameter | X-ray[24] | electron diffraction[25] | HF | HF/DFT (B3LYP) | DFT (BLYP) |
|---|---|---|---|---|---|
| Sn−Cl | 2.430(2) | 2.351(7) | 2.424 | 2.444 | 2.462 |
| Sn−C(1) | 2.121(8) | 2.106(6) | 2.121 | 2.130 | 2.145 |
| Sn−C(2) | 2.126(7) | 2.106(6) | 2.121 | 2.130 | 2.145 |
| Sn−C(3) | 2.109(7) | 2.106(6) | 2.121 | 2.130 | 2.145 |
| Cl−Sn−C(1) | 100.6(2) | 103.2(6) | 104.6 | 104.7 | 104.8 |
| Cl−Sn−C(2) | 99.1(2) | 103.2(6) | 104.6 | 104.8 | 104.8 |
| Cl−Sn−C(3) | 100.1(2) | 103.2(6) | 104.6 | 104.7 | 104.8 |
| C(1)−Sn−C(2) | 119.8(3) | 115(2) | 113.9 | 113.8 | 113.7 |
| C(1)−Sn−C(3) | 116.3(3) | 115(2) | 113.9 | 113.7 | 113.8 |
| C(2)−Sn−C(3) | 115.2(3) | 115(2) | 113.9 | 113.8 | 113.7 |

independent molecules of **4**, labeled *a* and *b*, and half a chloroform molecule. The single residual electron density peak of 1.84 e $Å^{-3}$ was located in the vicinity of the chloroform molecule; however, attempts to refine this as a disordered site did not improve the model.

**[$Me_2SnCl_2$(phen)] (5).** Colorless crystals were obtained from the slow evaporation of an acetonitrile solution of the adduct, prepared as for **3** using [$Me_2SnCl_2$] (Aldrich) and 1,10-phenanthroline; mp 264 (dec) °C. The choice of space group as *Cmcm*, as opposed to noncentrosymmetric $Cmc2_1$, was confirmed by the distribution of *E* statistics and the successful refinement. Thus, the tin atom lies on a site of symmetry *m*2*m*. Some disorder in the structure is evident, as can be seen from the shapes of the thermal displacement parameters of atoms comprising the 1,10-phenanthroline ligand; these were not considered sufficient, however, to reduce the symmetry of the space group.

## 3. Justification of Theoretical Model

The study has been conducted at the HF/LanL2DZ level of theory incorporating the use of the effective core potential (ECP)[11] approximation in the treatment of the tin atoms. As the Hartree−Fock (HF) approach makes no account of electron correlation in the reported geometry optimizations, it was thought desirable to conduct a comparative study using density functional theory (DFT) to confirm the validity of our approach. Thus, geometry optimization calcualtions have been conducted on two relatively small organotin systems, namely, [$MeSnCl_3$] and [$Me_3SnCl_3$] using the LanL2DZ basis set at the HF, B3LYP (a combination of HF/DFT), and BLYP (DFT) levels of theory. The advantage of investigating these systems is that both crystal structures[23,24] and gas-phase structures,[25] as determined by electron diffraction methods, are available and therefore a full comparison may be made between experimentally and theoretically determined geometries.

**3.1. [$MeSnCl_3$].** The crystal structure of [$MeSnCl_3$] shows that the tin atom exists in a distorted tetrahedral geometry and that the molecule possesses crystallographic $C_s$ symmetry and approximates $C_{3v}$ symmetry.[23] The gas-phase structure is $C_{3v}$.[25] Geometric parameters for both the solid-state and gas-phase structures are collected in Table 2. In addition to the symmetrization of the structure in the gas-phase compared with the solid-state structure, there is a general increase in the Sn−ligand bond distances in the absence of crystal packing effects. The optimized structures have been determined using the three levels of theory, and selected parameters are given in Table 2. Geometry optimization starting from coordinates derived from both the X-ray and electron diffraction studies coverged to the same optimized geometry regardless of the level of theory. The optimized structures resemble the experimentally determined gas-phase structure and all are characterized by an elongation of the Sn−ligand bond distances with the greatest elongation occurring at the DFT level of theory.

**3.2. [$Me_3SnCl$].** The crystal structure of [$Me_3SnCl$] shows a distorted tin atom geometry with the presence of intermolecular Sn···Cl interactions contributing to this distortion. Indeed, if the weaker Sn···Cl interactions were included in the coordination geometry, the structure would be described as polymeric with distorted trigonal-bipyramidal tin atom geometries.[24] The gas-phase structure is monomeric, $C_{3v}$.[25] By contrast to that observed in [$MeSnCl_3$], there is a general decrease in Sn−ligand parameters on going from the solid-state to the gas-phase structure. This can be readily rationalized in terms of the intermolecular Sn···Cl interactions cited above which are absent in the gas phase. A similar trend in elongation is found in the Sn−ligand parameters as the level of theory is modified from HF to DFT. Geometric parameters are listed in Table 3.

**3.3. General Comments.** The HF, HF/DFT, and DFT levels of theory result in essentially the same, symmetrical structures with an elongation in the Sn−ligand bond distances compared with the experimentally determined structures of [$MeSnCl_3$] with the deviation being greatest for the DFT theory. In [$Me_3SnCl$], analogous differences between the experimentally determined gas-phase structure and the optimized structures are noted. Thus, it may be stated that for the present study, for which the emphasis is on molecular geometry, the HF level of theory employing the LanL2DZ basis set is appropriate.

## 4. Results and Discussion

This study has examined the relationship between solid-state structures of certain diorganotin systems, as determined by X-ray crystallographic techniques, and their gas-phase structures employing ab initio geometry optimization calculations. It is noted that geometric changes are evident once a molecule's structure was calculated in the gas phase and, hence, free from the influence of crystal packing. The major observation was that the molecules became more symmetric in the gas phase. In terms of interatomic parameters, significant differences were noted in Sn−ligand parameters which were found to generally increase. Notable also was the observation that, generally, bond angles did not alter significantly. From the above, clearly, crystal packing effects can influence molecular geometry in diorganotin systems. Alternatively, it can be stated that the magnitude of energy associated with intermolecular interactions can be such as to induce changes in intramolecular interactions. The comparison between the crystallographically determined and theoretically calculated structures for five diorganotin systems is presented below.

**4.1. $[Ph_2Sn(S_2CNEt_2)_2]$ (1).** The first study examines the relationship between two polymorphic forms of $[Ph_2Sn(S_2CNEt_2)_2]$ (**1**) and their theoretically optimized structure. In

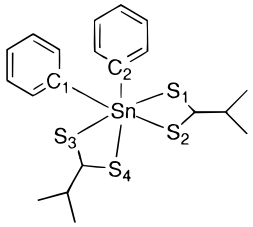


**1**

this context, a polymorph is defined as a material with essentially the same molecular structure but existing in a distinct crystal environment, i.e., a different (at least) arrangement of intermolecular forces.

$[Ph_2Sn(S_2CNEt_2)_2]$ (**1**) crystallizes as two polymorphs, namely monoclinic $P2_1/c$[26] and tetragonal $P4_12_12$.[27] The monoclinic form has been the subject of two independent crystal structure determinations on samples recrystallized from methyl ethyl ketone[26a] and ethanol/dichloromethane[26b] solutions of the compound, respectively, and the more contemporary results[26b] are employed here; similar unit cell data have been obtained for crystals obtained from recrystallization from acetone and $CHCl_3$ solutions of **1**.[27] The tetragonal form of **1** requires the molecule to possess crystallographically imposed 2-fold symmetry; crystallization of **1** from an acetonitrile/dichloromethane (1/1) solution gave similar unit-cell data.[27] The structure of **1** is unusual among compounds of the general formula $R_2Sn(S_2CNR'_2)_2$, which generally adopt skew-trapezoidal bipyramidal geometries owing to the presence of asymmetrically chelating dithiocarbamate ligands (i.e., Sn−S distances of approximately 2.5 and 3.0 Å) and in which the R substituents are disposed over the weaker Sn−S bonds.[1e] In **1**, a more symmetrical arrangement is found owing to the relatively near equivalence of the Sn−S bonds. Thus, the tin atom in each polymorphic form of **1** exists in a distorted octahedral geometry defined by two ipso carbon atoms of the phenyl groups that occupy approximately cis positions and four sulfur atoms derived from the two ligands.

There are no significant intermolecular contacts in the respective crystal lattices. In tetragonal **1**, the closest contact involving non-hydrogen atoms of 3.59(1) Å occurs between carbon atoms derived from the dithiocarbamate ligands and in monoclinic **1**, there are no non-hydrogen contacts < 3.6 Å. There are some significant differences in the geometric parameters about the tin centers in each polymorphic form of **1** as can be evidenced from the selected interatomic parameters collected in Table 4.

The dithiocarbamate ligands in tetragonal **1** form slightly asymmetric Sn−S distances such that ΔSn−S (i.e., $Sn-S_{long} - Sn-S_{short}$) is 0.103 Å, with an average Sn−S bond distance of 2.608 Å.[27] By contrast, in monoclinic **1** one dithiocarbamate ligand forms effectively symmetric Sn−S distances (ΔSn−S is 0.027 Å) and the other is more asymmetric with ΔSn−S of 0.219 Å; the average Sn−S distance is 2.644 Å.[26b] There is a high degree of agreement between the bond angles in the two polymorphs with the notable exception of a few angles involving the S(1) atom where differences of up to 7.3° exist. The geometry optimizations of tetragonal and monoclinic **1**, starting with the crystallographically determined fractional atomic coordinates, were performed in order to determine whether the different molecular structures found in the polymorphs of **1** arose as a result of crystal packing effects.

**TABLE 4: Geometric Parameters (Å, deg) and Calculated Energies (hartrees) for $[Ph_2Sn(S_2CNEt_2)_2]$ (1)**

| parameter | X-ray (tetragonal polymorph[27])[a] | X-ray (monoclinic polymorph[26b]) | optimized (LanL2DZ) |
|---|---|---|---|
| Sn−S(1) | 2.556(2) | 2.607(3) | 2.633 |
| Sn−S(2) | 2.659(2) | 2.632(3) | 2.840 |
| Sn−S(3) | 2.556(2) | 2.558(3) | 2.633 |
| Sn−S(4) | 2.659(2) | 2.777(3) | 2.840 |
| Sn−C(1) | 2.148(7) | 2.155(9) | 2.134 |
| Sn−C(2) | 2.148(7) | 2.166(8) | 2.134 |
| S(1)−Sn−S(2) | 67.91(6) | 68.2(1) | 66.9 |
| S(1)−Sn−S(3) | 150.08(7) | 155.3(1) | 149.6 |
| S(1)−Sn−S(4) | 88.67(7) | 96.0(1) | 89.5 |
| S(1)−Sn−C(1) | 95.4(2) | 93.9(2) | 96.5 |
| S(1)−Sn−C(2) | 103.5(2) | 98.9(2) | 102.0 |
| S(2)−Sn−S(3) | 88.67(7) | 90.7(1) | 89.5 |
| S(2)−Sn−S(4) | 78.72(9) | 81.0(1) | 80.8 |
| S(2)−Sn−C(1) | 160.9(2) | 158.0(2) | 160.6 |
| S(2)−Sn-C(2) | 92.2(2) | 93.9(2) | 89.4 |
| S(3)−Sn−S(4) | 67.91(6) | 67.0(1) | 66.9 |
| S(3)−Sn−C(1) | 103.5(2) | 103.0(2) | 102.0 |
| S(3)−Sn−C(2) | 95.4(2) | 95.2(2) | 96.5 |
| S(4)−Sn−C(1) | 92.2(2) | 88.6(2) | 89.4 |
| S(4)−Sn−C(2) | 160.9(2) | 161.2(2) | 160.6 |
| C(1)−Sn−C(2) | 101.1(4) | 101.8(3) | 104.5 |
| C(1)/Sn/C(2)/C(21) | 122.0(6) | −83 | −39.5 |
| C(1)/Sn/C(2)/C(26) | −58.2(7) | 91 | 140.3 |
| C(2)/Sn/C(1)/C(11) | 122.0(6) | 65 | 140.3 |
| C(2)/Sn/C(1)/C(16) | −58.2(7) | −110 | −39.5 |
| calcd energies | −1001.6459 | −1001.5889 | −1002.0139 |

[a] Molecule has crystallographic 2-fold symmetry.

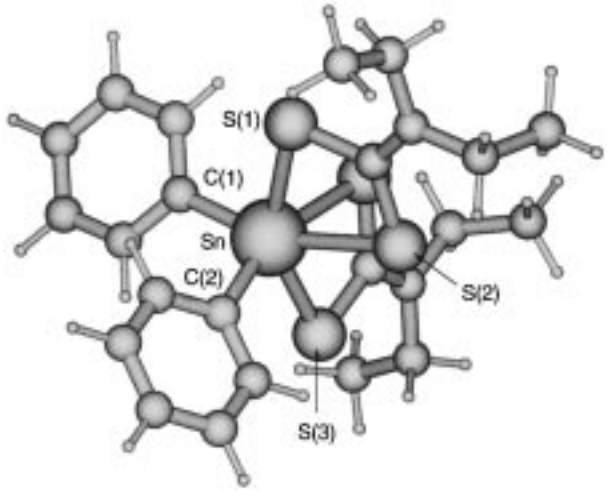


**Figure 1.** Optimized geometry for $[Ph_2Sn(S_2CNEt_2)_2]$ (**1**).

The geometry optimizations converged to the same structure as illustrated in Figure 1; interatomic parameters are listed in Table 4. The tetragonal form of **1** was determined to be (i) 966.2 kJ $mol^{-1}$ higher in energy than the optimized structure and (ii) more stable than the monoclinic form by 175.8 kJ $mol^{-1}$. The result that there is only one optimized, i.e., gas-phase structure, indicates that there is no intrinsic reason for **1** to exist as two distinct molecular structures, and hence any differences between the solid-state polymorphs can be related to intermolecular forces.

The optimized structure has effective 2-fold symmetry as is crystallographically imposed in the crystal structure of tetragonal **1**.[27] The average Sn−S distance has expanded to 2.737 Å, ΔSn−S is 0.207 Å, and the angles show a high level of agreement with those of tetragonal **1**, reflecting the 2-fold symmetry in the tetragonal polymorph (crystallographically

**TABLE 5: Geometric Parameters (Å, deg) and Calculated Energies (hartrees) for [$^t$Bu$_2$Sn(S$_2$CNcHex$_2$)Cl] (2)**

| parameter | X-ray (molecule *a*) | X-ray (molecule *b*) | optimized (LanL2DZ) (molecule *a*) | optimized (LanL2DZ) (molecule *b*) |
|---|---|---|---|---|
| Sn−Cl(1) | 2.482(3) | 2.492(3) | 2.485 | 2.486 |
| Sn−S(1) | 2.471(3) | 2.477(3) | 2.556 | 2.557 |
| Sn−S(2) | 2.722(3) | 2.743(3) | 2.960 | 2.957 |
| Sn−C(1) | 2.19(1) | 2.19(1) | 2.177 | 2.177 |
| Sn−C(5) | 2.16(1) | 2.21(1) | 2.177 | 2.177 |
| S(1)−C(9) | 1.740(9) | 1.73(1) | 1.814 | 1.805 |
| S(2)−C(9) | 1.71(1) | 1.72(1) | 1.771 | 1.779 |
| N(1)−C(9) | 1.31(1) | 1.31(1) | 1.318 | 1.318 |
| Cl−Sn−S(1) | 83.9(1) | 85.0(1) | 85.7 | 85.6 |
| Cl−Sn−S(2) | 152.0(1) | 152.3(1) | 151.1 | 151.0 |
| Cl−Sn−C(1) | 96.4(3) | 96.3(4) | 99.6 | 99.9 |
| Cl−Sn−C(5) | 98.6(3) | 96.9(3) | 99.9 | 99.6 |
| S(1)−Sn−S(2) | 68.04(8) | 67.50(9) | 65.4 | 65.4 |
| S(1)−Sn−C(1) | 115.3(4) | 120.1(4) | 116.0 | 115.9 |
| S(1)−Sn−C(5) | 119.8(4) | 113.5(4) | 115.9 | 116.0 |
| S(2)−Sn−C(1) | 95.1(3) | 95.2(4) | 93.4 | 93.2 |
| S(2)−Sn−C(5) | 96.0(3) | 96.6(3) | 93.2 | 93.5 |
| C(1)−Sn−C(5) | 123.9(5) | 125.6(6) | 125.4 | 125.4 |
| Sn−S(1)−C(9)−S(2) | 9.6(5) | −8.9(6) | 0.1 | 0.1 |
| Sn−S(1)−C(9)−N(1) | −170.5(8) | 173.1(9) | 0 | 179.9 |
| Sn−S(2)−C(9)−N(1) | 171.3(4) | −173.9(9) | 0 | 0 |
| C(9)−N(1)−C(10)−C(11) | 73(1) | −130(1) | 65.2 | −116.5 |
| C(9)−N(1)−C(10)−C(15) | −57(1) | 102(1) | −65.2 | 116.4 |
| C(9)−N(1)−C(16)−C(17) | −134.1(9) | 75(1) | −116.4 | 65.4 |
| C(9)−N(1)−C(16)−C(21) | 98(1) | −56(1) | 116.4 | −65.4 |
| calcd energies | −910.0397 | −910.0337 | −910.51223 | −910.51253 |

imposed) and the optimized gas-phase structure. The Sn−C distances appear to be shorter in the optimized structure; however, the relatively high errors with the crystallographically determined Sn−C bond distances must be noted. It is noteworthy that the dihedral angles between the phenyl groups are twisted in the following order: optimized structure > tetragonal **1** > monoclinic **1**; see Table 4. The reason for the elongation of the Sn−S distances in monoclinic **1** over those in tetragonal **1** can be rationalized in terms of the magnitude of the $\pi$-interactions between the phenyl groups. In the monoclinic polymorph, the phenyl groups are almost antiparallel, with an average twist of approximately 13°, indicating a relatively small interaction between the two $\pi$-systems. This contrasts to a larger twist of approximately 32° as observed in the structure of tetragonal **1**. An increase in the interaction between the phenyl $\pi$-systems reduces the electron density available to the tin atom and consequently results in the formation of stronger Sn−S interactions. Hence, it may be concluded that the chief influence of the crystal packing in the two polymorphs of **1** is to alter the relative positions of the phenyl groups, which in turn influences the geometric parameters about the tin atom. The dihedral angles are quite similar for the optimized structure (approximately 40°) and tetragonal **1**, and thus the expansion in the Sn−S bond distances between the two solid-state structures reflects the influence of the different intermolecular forces operating in the polymorphs of **1**.

**4.2. [$^t$Bu$_2$Sn(S$_2$CNcHex$_2$)Cl] (2).** The structure of [$^t$Bu$_2$Sn(S$_2$CNcHex$_2$)Cl] (**2**) is an example of a compound with two formula units comprising the crystallographic asymmetric unit. Thus, while there will be different intermolecular interactions operating on each molecule, as found for the polymorphs of **1**, the molecules are constrained within a single unit cell.

The molecular structures for the two formula units that comprise the crystallographic asymmetric unit of **2**, labeled molecules *a* and *b*, are shown in Figure 2, and selected interatomic parameters are collected in Table 5. The tin atom is five-coordinate being bonded to two *tert*-butyl groups, a chloride and two sulfur atoms derived from an asymmetrically chelating dithiocarbamate ligand. The geometry is distorted trigonal bipyramidal with the axial sites being defined by the chloride and the less tightly bound S(2) atom. The tin atom

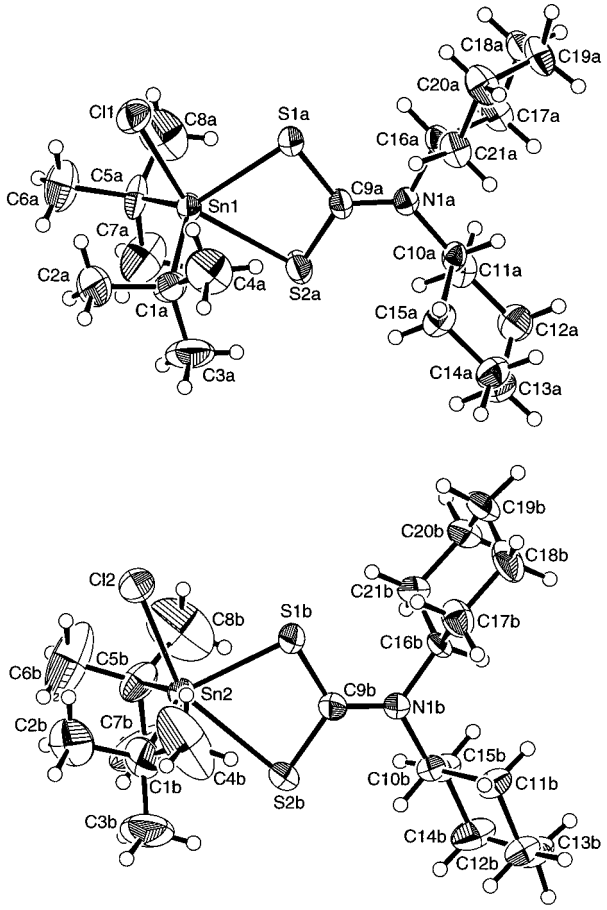


**Figure 2.** Molecular structures for the two independent molecules of [$t$Bu$_2$Sn(S$_2$CNcHex$_2$)Cl] (**2**) showing the crystallographic numbering scheme employed.

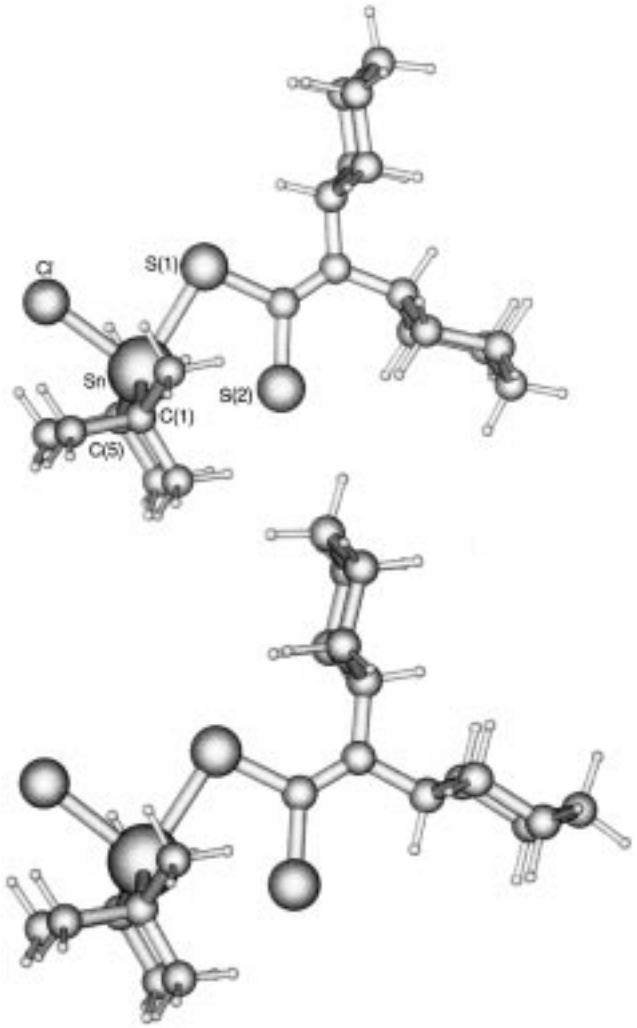


**Figure 3.** Optimized geometries for [$^t$Bu$_2$Sn(S$_2$CNcHex$_2$)Cl] (**2**) highlighting the pseudo-mirror relationship between the pairs of N-bound cyclohexyl rings (upper view: molecule *a*).

lies 0.1270(6) Å (0.1191(7) Å for molecule *b*) out of the trigonal $C_2S(1)$ plane in the direction of the chloride atom. As can be seen from the listed parameters in Table 5, there are only minor differences between the two independent molecules with the greatest difference in bond distances involving the Sn−S(2) interactions. The difference between the molecules relates to the relative positions of the cyclohexyl groups.

Molecular models of the two independent molecules shows that the $^t$Bu$_2$SnCl(S$_2$CN) portions of each molecule are virtually superimposable; however, the cyclohexyl portions are not, as they are approximate mirror images of each other. Hence, the differences between the two molecules relate to conformation rather than to disparate interatomic parameters. In the lattice the closest contact occurs between symmetry related C(19) atoms of 3.60(2) Å (symmetry operation: $2 - x, -y, 1 - z$). Both molecules that comprise the crystallographic unit in **2** were subjected to a geometry optimization.

Geometry optimizations of the two crystallographically independent molecules of **2**, i.e., *a* and *b*, were performed in order to ascertain whether the distinct structures were in fact isomers or were due to crystal packing effects. The energy minimized structures determined for **2** are illustrated in Figure 3 and show that the two molecules are indeed isomers. The geometry optimizations converged to different structures, i.e., molecule *a* (upper view of Figure 3) and molecule *b*. The energy difference between the two computed structures is negligibly small. As such, it is possible that normally acceptable criteria describing geometric convergence masked the identity of a single, globally minimized molecular geometry. Accordingly, geometry optimizations were repeated with tighter convergence criteria. The additional calculations confirmed the presence of two distinct structures, with a difference in energy between them of 0.8 kJ mol$^{-1}$. In terms of overall conformation, the major difference between the crystallographic geometries and the geometry-optimized structures relates to the relative orientations of the N-bound cyclohexyl rings. It was noted above that in the solid state the cyclohexyl portions of the molecules could be related to each other by a pseudo-mirror plane. It is interesting in this context that the starting geometries converged not to a single structure but to two distinct structures in which the pseudo-mirror relationship has been maintained and, indeed, tightened; this is reflected in the equivalence of the C−N−C−C torsion angle data (Table 5) and is emphasized in Figure 3. The small (negligible) energy difference between the two optimized structures indicates that the structures are effectively isomers. Accordingly, there are no significant differences between the parameters describing the tin atom geometries in the optimized structures. Comparing the parameters for the gas-phase and solid-state structures, however, reveals a number of interesting trends.

There is a considerable expansion in the Sn−S separations but not so for the Sn−Cl distances suggesting that the Sn−Cl interaction is stronger in the gas-phase structure compared with the solid-state structure; differences in the Sn−C separations are marginal. This result could suggest that the dithiocarbamate ligand has more ionic character in the gas phase. Generally, there are few significant differences in bond angles between the solid-state and gas-phase structures. In terms of energy considerations, it has already been mentioned that the difference in energy between the optimized structures was found to be only 0.8 kJ mol$^{-1}$. Comparing the gas-phase to the solid-state structures shows that the optimized structure for molecule *a* was 1240.6 kJ mol$^{-1}$ more stable than the molecular structure in the solid state and the comparable value for molecule *b* was calculated to be 1257.1 kJ mol$^{-1}$. These values indicate that there is a chemically significant difference of 15.8 kJ mol$^{-1}$ between the two molecules comprising the crystallographic asymmetric unit.

**4.3. [Vin$_2$SnCl$_2$(bipy)]·0.5C$_6$H$_6$ (3).** An analysis of [Vin$_2$SnCl$_2$(bipy)] (**3**) was performed as the molecule crystallizes with occluded solvent molecules in the lattice, and it was thought of interest to ascertain what extent noncoordinating solvent can influence molecular geometry.

The molecular structure of [Vin$_2$SnCl$_2$(bipy)] (**3**), determined as its hemi-benzene solvate (situated about a crystallographic center of inversion), is shown in Figure 4, and selected geometric parameters are collected in Table 6. The tin atom exists in a distorted octahedral geometry with the tin atom 0.0114(7) Å above the $N_2Cl_2$ plane in the direction of the C(1) atom. The vinyl groups occupy trans positions and the dihedral angle between the $SnC_2$ planes is 152.0°, indicating that the vinyl groups are not coplanar; the C(2)−C(1)−C(3)−C(4) torsion angle is −29.7(9)°.

In the lattice, the benzene molecules occupy columns that run parallel to the crystallographic *c*-axis; a view of the unit-cell contents, projected down the *c*-direction, is shown in Figure 5. The closest non-hydrogen contact in the lattice of 3.473(6) Å occurs between the C(11) and C(13)$^i$ atoms (symmetry operation *i*: $-x, 1 - y, 1 - z$). This contact is one of several (the next closest is 3.560(6) Å) that arise as a result of the

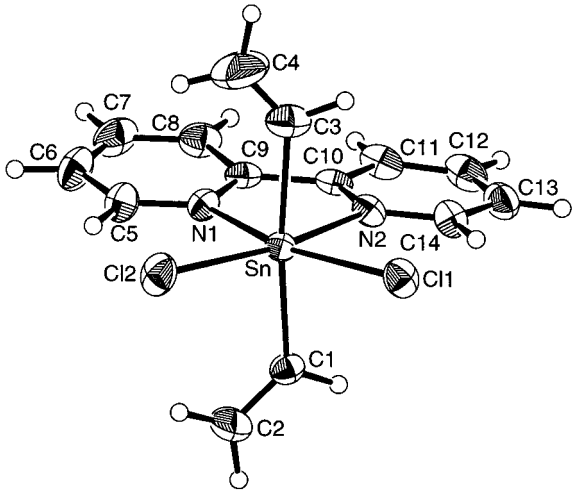


**Figure 4.** Molecular structure for $[Vin_2SnCl_2(bipy)]$ (**3**) showing the crystallographic numbering scheme employed.

**TABLE 6: Geometric Parameters (Å, deg) and Calculated Energies (hartrees) for $[Vin_2SnCl_2(bipy)]\cdot 0.5C_6H_6$ (3)**

| parameter | X-ray | optimized (LanL2DZ) |
|---|---|---|
| Sn−Cl(1) | 2.529(1) | 2.525 |
| Sn−Cl(2) | 2.463(1) | 2.525 |
| Sn−N(1) | 2.360(3) | 2.404 |
| Sn−N(2) | 2.396(3) | 2.404 |
| Sn−C(1) | 2.119(3) | 2.111 |
| Sn−C(3) | 2.119(4) | 2.111 |
| Cl(1)−Sn−Cl(2) | 104.74(3) | 109.7 |
| Cl(1)−Sn−N(1) | 161.50(7) | 159.5 |
| Cl(1)−Sn−N(2) | 92.47(7) | 90.8 |
| Cl(1)−Sn−C(1) | 89.71(9) | 91.3 |
| Cl(1)−Sn−C(3) | 89.2(1) | 94.4 |
| Cl(2)−Sn−N(1) | 93.72(7) | 90.8 |
| Cl(2)−Sn−N(2) | 162.79(7) | 159.5 |
| Cl(2)−Sn−C(1) | 94.2(1) | 94.4 |
| Cl(2)−Sn−C(3) | 94.3(1) | 91.3 |
| N(1)−Sn−N(2) | 69.1(1) | 68.7 |
| N(1)−Sn−C(1) | 90.2(1) | 86.9 |
| N(1)−Sn−C(3) | 88.1(1) | 84.9 |
| N(2)−Sn−C(1) | 85.4(1) | 84.9 |
| N(2)−Sn−C(3) | 86.1(1) | 86.9 |
| C(1)−Sn−C(3) | 171.4(2) | 170.1 |
| C(1)/Sn/C(3)/C(4) | −54(6) | 121.4 |
| C(3)/Sn/C(1)/C(2) | 125(6) | 121.5 |
| calcd energies | −679.5857 | −679.7460 |

interlocking of centrosymmetrically related bipyridyl residues, also along the crystallographic *c*-direction, and is indicative of some $\pi$-stacking in the lattice. There are no non-hydrogen contacts less than the 3.6 Å involving **3** and the benzene molecules. The chloride atoms form a number of contacts with hydrogen atoms of adjacent columns with the closest involving the Cl(1) atom of 2.78 Å with H(8a)$^{ii}$ (symmetry operation *ii*: $1 + x, y, z$); the closest involving the Cl(2) atom is 2.94 Å with H(7a)$^{ii}$. Both chloride atoms form contacts with the solvent molecule with the closest of 2.90 Å involving Cl(1) and H(101); Cl(2) forms a contact of 3.40 Å with H(102)$^{iii}$ (symmetry operation *iii*: $x, y, -1 + z$). It is of interest that Cl(1) forms the two shortest Cl···H interactions and that it forms the longer of the Sn−Cl bonds, i.e., 2.529(1) Å, cf. 2.463(1) Å. In this context it is noteworthy that there are some close *intra*molecular Cl···H interactions as well. Thus, Cl(1) is separated by 2.81 Å from H(14a) and 3.11 Å from H(3a). By contrast, the Cl(2) atom forms two close contacts, one of 2.78 Å to H(5a) and 2.77 Å to H(2a). In the absence of other structural features, the disparity in the Sn−Cl distances and consequently, through

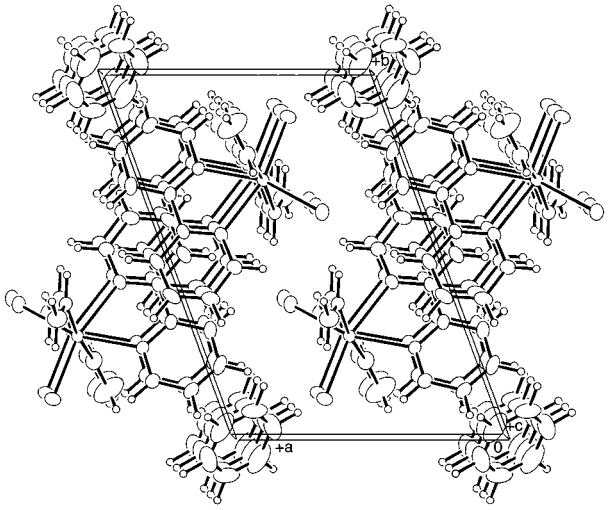


**Figure 5.** Unit-cell contents for $[Vin_2SnCl_2(bipy)]$ (**3**).

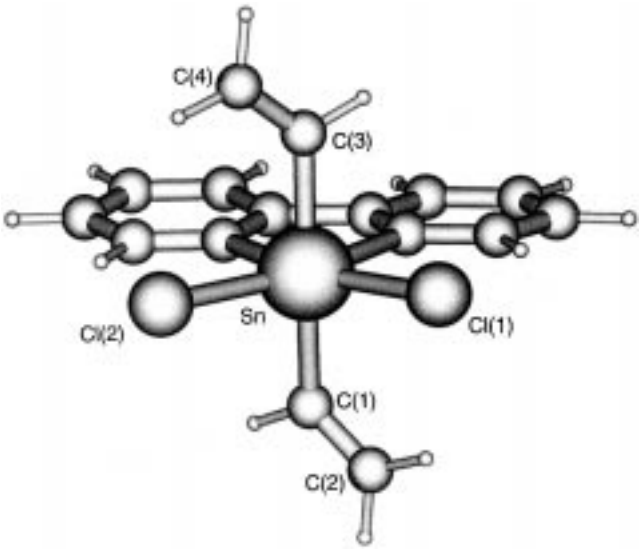


**Figure 6.** Optimized geometry for $[Vin_2SnCl_2(bipy)]$ (**3**).

the trans influence, the Sn−N distances (Table 6), may be ascribed to the intermolecular associations described above. To examine this hypothesis further, the geometry of **3** was subjected to a geometry optimization.

The optimized structure of **3** is shown in Figure 6, and derived geometric parameters are listed in Table 6. The most notable difference in the structure is the symmetrization that has occurred in the optimized geometry. There is a 2-fold axis of symmetry in the optimized structure of **3** with the axis bisecting the $SnCl_2N_2$ basal plane, passing through the Cl−Sn−Cl angle. Whereas in the solid state the terminal end of the vinyl substituents were found to lie on the same side of the molecule, in the optimized structure, the orientation of the vinyl groups is such that they each lie over a different Sn−Cl bond. In this arrangement, the Cl···H−C(5,14) separations are both 2.60 Å and Cl···H−C(2,4) is 2.79 Å. Thus, the major structural difference between the experimental and calculated structures is a rotation about a Sn−C bond. The symmetry in the molecule is reflected in the equivalence in the three pairs of Sn−donor atom distances (Table 4). For the optimized geometry there is an expansion in the Sn−Cl and Sn−N atom parameters but a small contraction in Sn−C bond lengths. It is noteworthy that the inequivalence in the Sn−Cl and Sn−N parameters found in the crystal structure no longer pertain in the gas-phase structure. This observation further supports the conclusion that

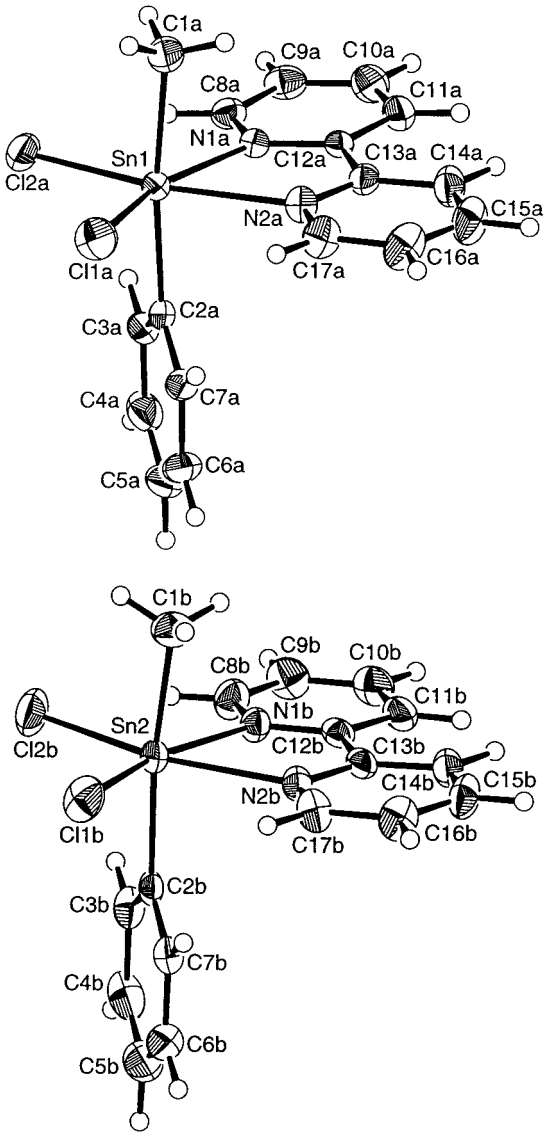


**Figure 7.** Molecular structures for the two independent molecules of [Me(Ph)$SnCl_2$(bipy)] (**4**) showing the crystallographic numbering scheme employed.

the differences that do exist in the solid state are due to intermolecular forces rather than any intrinsic chemistry associated with the molecule. In terms of bond angles, differences between equivalent angles in the solid state and calculated structures are in the order of 0−3° with the exception of the Cl(1)−Sn−Cl(2) and Cl(1)−Sn−C(3) angles, which have expanded by approximately 5° in the calculated structure.

The crystallographically determined structure (single-point calculation) was found to be 420.9 kJ $mol^{-1}$ higher in energy than the optimized structure.

**4.4. [Me(Ph)$SnCl_2$(bipy)]·0.25$CHCl_3$ (4).** The [Me(Ph)-$SnCl_2$(bipy)] (**4**) structure is an example where two independent molecules comprise the asymmetric unit in addition to occluded solvent. In this analysis the two effects examined earlier in **2** (two independent molecules) and **3** (occluded solvent) are combined in the one lattice.

Two molecules (labeled *a* and *b*) of [Me(Ph)$SnCl_2$(bipy)] and half a chloroform molecule comprise the crystallographic asymmetric unit of **4**. The overall geometry for **4** is, allowing for the necessary changes, is essentially as described above for **3**. From an inspection of the molecular structures illustrated in Figure 7 and the selected interatomic parameters collected in Table 7, it is clear that there are no major differences between the two independent molecules. There is a slight disparity in the Sn−Cl bond distances for molecule *b* that is not found for molecule *a*, and the greatest difference in bond angles between *a* and *b*, i.e., 4.2°, is found for the Cl(2)−Sn−N(1) angles. The tin atom lies 0.0091(4) Å [0.0166(5) Å for molecule *b*] above the $N_2Cl_2$ plane in the direction of the ipso carbon atom of the phenyl group. The orientation of the phenyl group with respect to the $N_2Cl_2$ plane is the same for the two molecules, i.e., the dihedral angle between the respective planes is 91.4° for both molecules, a result that emphasizes the similarity between their structures. There are differences, however, in the nature of their intermolecular associations.

**TABLE 7: Geometric Parameters (Å, deg) and Calculated Energies (hartrees) for [Me(Ph)$SnCl_2$(bipy)]·0.25$CHCl_3$ (4)**

| parameter | X-ray (molecule *a*) | X-ray (molecule *b*) | optimized (LanL2DZ) |
|---|---|---|---|
| Sn−Cl(1) | 2.488(2) | 2.500(2) | 2.536 |
| Sn−Cl(2) | 2.492(2) | 2.481(2) | 2.536 |
| Sn−N(1) | 2.389(5) | 2.388(5) | 2.404 |
| Sn−N(2) | 2.401(5) | 2.391(5) | 2.404 |
| Sn−C(1) | 2.139(7) | 2.110(8) | 2.115 |
| Sn−C(2) | 2.154(7) | 2.142(7) | 2.140 |
| Cl(1)−Sn−Cl(2) | 101.89(7) | 103.14(7) | 110.0 |
| Cl(1)−Sn−N(1) | 161.7(1) | 164.7(1) | 159.3 |
| Cl(1)−Sn−N(2) | 93.1(1) | 95.5(1) | 90.7 |
| Cl(1)−Sn−C(1) | 93.7(2) | 90.1(3) | 90.4 |
| Cl(1)−Sn−C(2) | 93.2(2) | 91.4(2) | 93.5 |
| Cl(2)−Sn−N(1) | 96.4(1) | 92.2(1) | 90.7 |
| Cl(2)−Sn−N(2) | 165.0(1) | 161.3(1) | 159.3 |
| Cl(2)−Sn−C(1) | 91.7(2) | 93.1(3) | 90.4 |
| Cl(2)−Sn−C(2) | 91.4(2) | 92.9(2) | 93.5 |
| N(1)−Sn−N(2) | 68.5(2) | 69.2(2) | 68.6 |
| N(1)−Sn−C(1) | 85.2(2) | 88.5(3) | 88.2 |
| N(1)−Sn−C(2) | 86.9(2) | 88.4(2) | 86.2 |
| N(2)−Sn−C(1) | 86.9(2) | 85.6(3) | 88.2 |
| N(2)−Sn−C(2) | 88.1(2) | 87.7(2) | 86.2 |
| C(1)−Sn−C(2) | 171.8(3) | 173.3(3) | 173.3 |
| C(1)/Sn/C(2)/C(3) | −72(2) | −120(3) | −90 |
| C(1)/Sn/C(2)/C(7) | 111(2) | 63(3) | 90 |
| calcd energies | −794.3827 | −794.3760 | −794.5436 |

The most significant contact in the lattice involving the tin-bound chloride atoms is 2.72 Å which occurs between Cl(1b) and H(100), i.e., the chloroform hydrogen; Cl(1b)···C(100) is 3.51(1) Å. The next closest contact of 2.87 Å also involves Cl(1b) [Cl(1b)···H(9a)$^{i}$; symmetry operation *i*: $0.5 - x$, $-0.5 + y$, $0.5 - z$] and all other contacts involving Sn−Cl are all longer than these and hence, it can be surmised that the elongation of the Sn(2)−Cl(1b) bond with respect to the other Sn−Cl bonds is due to intermolecular Cl···H interactions, as found in the structure of **3**. A number of further interactions between the solvent chloroform molecule exist with Cl(30)···H-(15b)$^{ii}$ (symmetry operation *ii*: $-0.5 + x$, $0.5 - y$, $0.5 + z$) of 2.79 Å being the closest. The closest non-hydrogen contact in the lattice is 3.43(1) Å and occurs between the C(9a) and C(15a)$^{iii}$ atoms (symmetry operation *iii*: $1 - x$, $1 - y$, $-z$). This separation is indicative of some $\pi-\pi$ interactions between centrosymmetrically pairs of molecule *a*; similar interactions of 3.44 Å are present for isolated pairs of molecule *b*. For **4**, there are two essentially identical molecules that differ only in their (weak) intermolecular contacts. Not surprisingly, geometry optimization calculations showed that both molecules converged to the same geometry, Figure 8, and a comparison between the experimentally determined structures and the energy minimized molecule reveals a number of notable trends.

As can be seen from Table 7, the Sn−Cl and Sn−N distances in the optimized structure are longer than those found in the

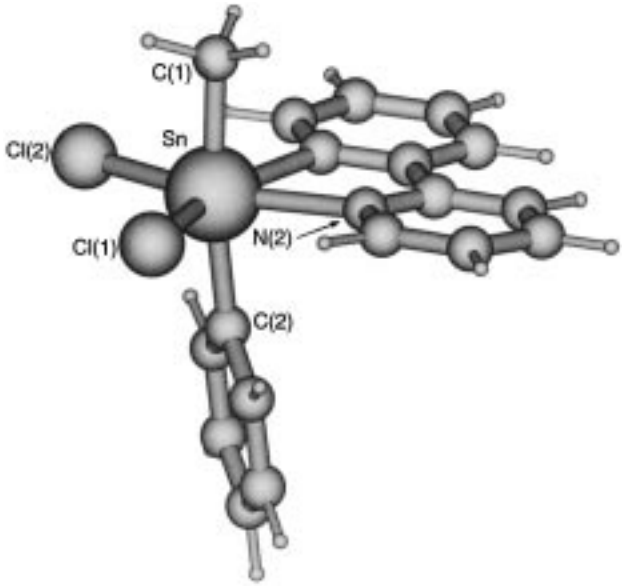


**Figure 8.** Optimized geometry for [Me(Ph)$SnCl_2$(bipy)] (**4**).

solid state. Comparison of Sn−C distances is problematic owing to the relatively high errors associated with these parameters; however, it is noteworthy that the Sn−C(methyl) distance in the optimized geometry is shorter than the Sn−C(phenyl) separation. In terms of angles, the greatest difference is found in the Cl−Sn−Cl angle which has expanded by ca. 8° and 7°, respectively, compared to molecules *a* and *b* in the solid state; there are concomitant changes in the other angles about the tin atom. In terms of overall geometry, the optimized structure is more symmetrical, having mirror symmetry, with equivalence between similar Sn−ligand bond distances and, allowing for chemistry, between comparable angles.

The single-point calculations based on the crystallographically determined structures of molecules *a* and *b* showed that molecule *a* was 17.6 kJ $mol^{-1}$ more stable than molecule *b*. Further, the optimized structure of molecule *a* was 422.4 kJ $mol^{-1}$ more stable than the crystallographic structure, and the comparable value for molecule *b* was 440.0 kJ $mol^{-1}$. It can be therefore concluded that the differences noted above between the two independent molecules comprising the crystallographic asymmetric unit of **4** can be attributed to crystal packing effects and in the absence of these effects, solid-state **4** converges to a single gas-phase structure.

**4.5. [$Me_2SnCl_2$(phen)] (5).** The final example for analysis is [$Me_2SnCl_2$(phen)] (**5**), which has crystallographic symmetry. A general feature of the crystallographically determined structures described above is a lack of symmetry in the molecule as found in the solid state and after geometry optimization, the symmetrization of the structure, often accompanied by a significant change in geometric parameters. Hence, differences between individual geometric parameters may reflect changes in geometry/conformation rather than crystal packing effects alone. The geometry optimization of **5** was conducted in order to examine what changes in geometric parameters are apparent when, presumably, only minor changes in geometry occur upon optimization as the starting geometry is already highly symmetric.

The molecular structure as determined by X-ray diffraction for **5** is shown in Figure 9, and selected interatomic parameters are collected in Table 8. The tin atom lies on a crystallographic site of symmetry *m*2*m* with one mirror plane being defined by the chloride atoms and the phenanthroline ligand, another by

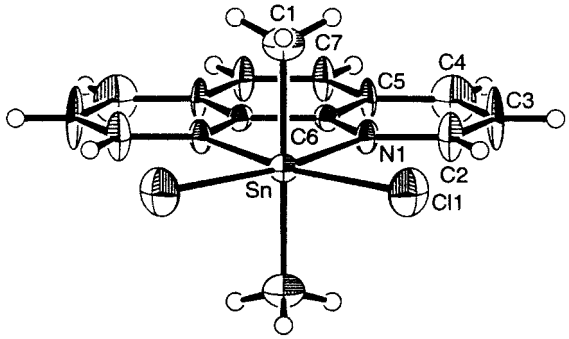


**Figure 9.** Molecular structure for [$Me_2SnCl_2$(phen)] (**5**) showing the crystallographic numbering scheme employed.

**TABLE 8: Geometric Parameters (Å, deg) and Calculated Energies (hartrees) for [$Me_2SnCl_2$(phen)] (5)**

| parameter | X-ray[a] | optimized (LanL2DZ) |
|---|---|---|
| Sn−Cl(1) | 2.521(3) | 2.550 |
| Sn−Cl(2) | 2.521(3) | 2.550 |
| Sn−N(1) | 2.385(9) | 2.419 |
| Sn−N(2) | 2.385(9) | 2.419 |
| Sn−C(1) | 2.075(8) | 2.113 |
| Sn−C(2) | 2.075(8) | 2.113 |
| Cl(1)−Sn−Cl(2) | 106.1(1) | 111.9 |
| Cl(1)−Sn−N(1) | 92.6(3) | 89.5 |
| Cl(1)−Sn−N(2) | 161.3(3) | 158.6 |
| Cl(1)−Sn−C(1) | 90.7(1) | 91.1 |
| Cl(1)−Sn−C(2) | 90.7(1) | 91.1 |
| Cl(2)−Sn−N(1) | 161.3(3) | 158.6 |
| Cl(2)−Sn−N(2) | 92.6(3) | 89.5 |
| Cl(2)−Sn−C(1) | 90.7(1) | 91.1 |
| Cl(2)−Sn−C(2) | 90.7(1) | 91.1 |
| N(1)−Sn−N(2) | 68.7(5) | 69.2 |
| N(1)−Sn−C(1) | 89.1(1) | 88.4 |
| N(1)−Sn−C(2) | 89.1(1) | 88.4 |
| N(2)−Sn−C(1) | 89.1(1) | 88.4 |
| N(2)−Sn−C(2) | 89.1(1) | 88.4 |
| C(1)−Sn−C(2) | 177.8(4) | 176.0 |
| calcd energies | −679.6752 | −679.8329 |

[a] Molecule has *m*2*m* symmetry such that Cl(1) = Cl(2), N(1) = N(2), and C(1) = C(2).

the methyl carbons (and two of the hydrogen atoms) and tin atom; the 2-fold axis passes through the tin atom and bisects the Cl···Cl and N···N vectors. The overall structure is similar to that described above for **3** and **4**. The closest non-hydrogen atom contact in the lattice is 3.39(2) Å, and this occurs between two $C(1)^i$ atoms (symmetry operation *i*: $+x, +y, 1.5 - z$). The closest contact involving chloride is 2.81 Å with $H(4)^{ii}$ (symmetry operation *ii*: $0.5 - x, -0.5 - y, 0.5 + z$).

Optimized parameters for **5** are listed in Table 8 and the geometry is illustrated in Figure 10. The key result of the calculation is that there has been a uniform elongation in the tin−ligand parameters with Sn−Cl, Sn−N, and Sn−C distances each elongating by 0.029, 0.034, and 0.038 Å, respectively. The major difference among the angles is the expansion of the Cl−Sn−Cl angle from 106.1(1)° in the crystal structure to 111.9° in the optimized structure.

The difference in energy between the experimentally observed and optimized structures was found to be 414.1 kJ $mol^{-1}$, the latter being more stable.

## 5. Energy Considerations

When considering energy differences calculated between single-point and geometry-optimized structures, one needs to be wary as errors in crystal structure determination can vary

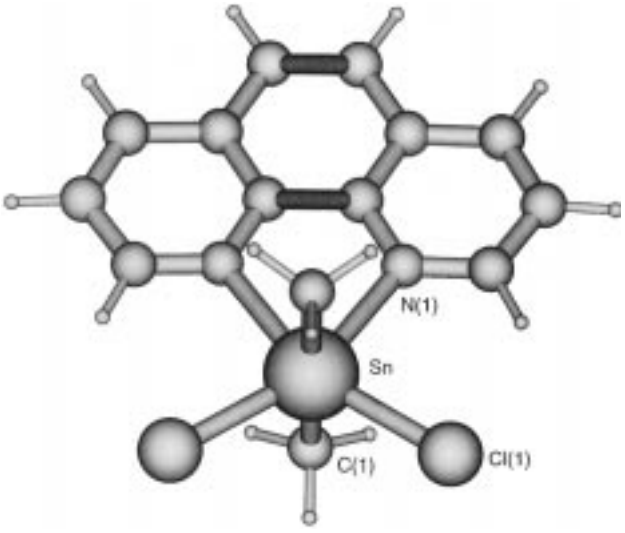


**Figure 10.** Optimized geometry for $[Me_2SnCl_2(phen)]$ (**5**).

from system to system. Minor conformational differences and disorder (positional and thermal) can give rise to different energies. One obvious source of error concerns the treatment of hydrogen atoms which are normally included in their calculated positions in crystallographic refinements at 0.95−1.0 Å in order to model electron density maxima. In the optimized geometries the C−H distances were 1.07−1.08 Å. As a trial, three separate single-point calculations were conducted for molecule *a* of **2** in which the hydrogen atoms were included at C−H separations of 0.90, 0.97, and 1.08 Å. The energy calculated for the structure with the longer C−H separations was found to be 608.8 kJ $mol^{-1}$ more stable than the structure with C−H constrained to 0.97 Å, and this was, in turn, 519.3 kJ $mol^{-1}$ more stable than the structure with C−H constrained to 0.90 Å. Clearly, the treatment of hydrogen atoms in the X-ray experiment significantly influences the energy differences calculated for the molecules. The above calculations reveal that the treatment of hydrogen atoms in the X-ray experiment may account for approximately 30% of the energy difference between the experimental and calculated structures.

It should be noted that free energy differences calculated for polymorphs of organic compounds are estimated to be in the order of 4−8 kJ $mol^{-1}$.[28] Higher energies would be expected for the larger systems (in terms of both atoms sizes and numbers of atoms) described in the present study; however, it is certain that the energy differences calculated between the solid-state and gas-phase structures are overestimated.

We do not believe that conclusions drawn from our energy analyses are seriously affected by possible overestimations brought about by the lack of electron correlation in our calculations. Incorporation of electron correlation will not significantly alter the semiquantitative conclusion drawn here that, relative to the experimentally determined crystal structures, the more symmetric isolated molecular configurations are more stable by chemically significant amounts of energy. Support for this conclusion is found by referring back to the energy differences calculated for the structures reported in section 3.

Table 9 lists the single-point energies calculated for $[MeSnCl_3]$ and $[Me_3SnCl]$ employing the LanL2DZ basis set at the HF, HF/DFT (B3LYP), and DFT (BLYP) levels of theory starting from the X-ray determined coordinates and those obtained from the electron diffraction studies. It is noteworthy that both starting points converged to the same optimized geometry for each of the levels of theory. In terms of energy considerations

**TABLE 9: Calculated Energies (hartrees) for $[MeSnCl_3]$ and $[Me_3SnCl]$ Employing the LanL2DZ Basis Set at the HF, HF/DFT, and DFT Levels of Theory**

| | HF | HF/DFT (B3LYP) | DFT (BLYP) |
|---|---|---|---|
| $[MeSnCl_3]$ | | | |
| single point | | | |
| X-ray coordinates[23] | −87.0568 | −88.0251 | −88.0202 |
| electron diffraction coordinates[25] | −87.1045 | −88.2567 | −88.0835 |
| optimized geometry | −87.1092 | −88.2638 | −88.0935 |
| $[Me_3SnCl]$ | | | |
| single point | | | |
| X-ray coordinates[24] | −136.6858 | −137.9594 | −137.7910 |
| electron diffraction coordinates[25] | −136.8165 | −138.1110 | −137.9553 |
| optimized geometry | −136.8305 | −138.1206 | −137.9641 |

there are two key results. The first is that the energy difference between the optimized geometry and the experimental gas-phase structure is an order of magnitude less than the energy difference between the solid-state structure and optimized structure, clearly indicating an influence of crystal packing effect. The second noteworthy result for these systems is that the magnitude of energy differences between the experimental structures (determined either in the solid state or in the gas phase) is smallest at the HF level of theory compared with the other levels of theories investigated.

## 6. Conclusions

This combined crystallographic and theoretical study of selected organotin systems has addressed the question of whether crystal packing effects can significantly influence molecular geometry. It has been found that in the absence of crystal packing effects, the solid-state geometries uniformly converged to more symmetric structures, and hence it is possible to conclude that crystal packing effects can influence molecular geometry about heavy metal centers such as tin. It was also found that Sn−ligand bond distances generally increased but that bond angles did not change greatly apart from those involved in the symmetrization of the structure. In terms of energy differences, it may be concluded that the energy difference between molecules in two distinct crystalline environments (i.e., polymorphs) as calculated for **1** are greater than energy differences between two molecules that crystallize in the one lattice, e.g., **2** and **4**. Further, the presence of solvent in the lattice, as in **3** and **4**, does not markedly alter the energy differences calculated between the condensed and gas phases, allowing for different sizes of the molecules.

**Acknowledgment.** This work was supported by the Australian Research Council. Computing resources provided by the South Australian Centre for Parallel Computing (SACPC) are gratefully acknowledged. V.J.H. was the holder of a Commonwealth Postgraduate Research Award.

**Supporting Information Available:** Crystal and refinement data, list of atomic coordinates and thermal parameters, and all bond distances and angles for **2**−**5** (26 pages). Ordering information is given on any current masthead page.

## References and Notes

(1) (a) Haiduc, I.; Sowerby, D. B.; Lu, S.-F. *Polyhedron* **1995**, *14*, 3389. (b) Silvestru, C.; Haiduc, I. *Coord. Chem. Rev.* **1996**, *147*, 117. (c) Tiekink, E. R. T.; Winter, G. *Rev. Inorg. Chem.* **1992**, *12*, 183. (d) Tiekink, E. R. T. *Trends in Organomet. Chem.* **1994**, *1*, 71. (e) Tiekink, E. R. T.

*Main Group Met. Chem.* **1992**, *15*, 161. (f) Cox, M. J.; Tiekink, E. R. T. *Rev. Inorg. Chem.* **1997**, *17*, 1.

(2) Tiekink, E. R. T. *Acta Crystallogr. Sect. C* **1987**, *43*, 448.

(3) Hounslow, A. M.; Tiekink, E. R. T. *J. Cryst. Spectrosc. Res.* **1991**, *21*, 133.

(4) Watanabe, Y. *Acta Crystallogr. Sect. B* **1977**, *37*, 3566.

(5) (a) Davies, A. G.; Smith, P. J. In Wilkinson, G., Stone, F. G. A., Abel, E. W., Eds.; *Comprehensive Organometallic Chemistry*; Pergamon Press: Oxford, 1982; Vol. 2. (b) Blunden, S. J.; Chapman, A. In Craig, P. J., Ed.; *Organometallic Compounds in the Environment*; Longman, Harlow, 1986. (c) Champ, M. A.; Seligman, P. F. In Champ, M. A., Seligman, P. F., Eds.; *Organotin: Environmental Fate and Effects*; Chapman & Hall: London, 1996; Chapter 1. (d) Gielen, M. *Coord. Chem. Rev.* **1996**, *151*, 41.

(6) Burda, J. V.; Sponer, J.; Hobza, P. *J. Phys. Chem.* **1996**, *100*, 7250.

(7) Stewart, G. M.; Tiekink, E. R. T.; Buntine, M. A. *J. Phys. Chem. A* **1997**, *101*, 5368.

(8) Jiang, S.; Dasgupta, S.; Blanco, M.; Frazier, R.; Yamaguchi, E. S.; Tang, Y.; Goddard, W. A. *J. Phys. Chem.* **1996**, *100*, 15760.

(9) Frenking, G.; Pidun, U. *J. Chem. Soc., Dalton Trans.* **1997**, 1653.

(10) (a) Bernstein, J.; Hagler, A. T. *J. Am. Chem. Soc.* **1978**, *100*, 673. (b) Bernstein, J. *J. Phys. D: Appl. Phys.* **1993**, *26*, B66. (c) Dauber, P.; Hagler, A. T. *Acc. Chem. Res.* **1980**, *13*, 105. (d) Royer, J.; Décoret, C.; Tinland, B.; Perrin, M.; Perrin, R. *J. Phys. Chem.* **1989**, *93*, 3393. (e) Gavezzotti, A.; Filippini, G. *J. Phys. Chem.* **1995**, *117*, 12299.

(11) (a) Wadt, W. R.; Hay, P. J. *J. Chem. Phys.* **1985**, *82*, 270. (b) Wadt, W. R.; Hay, P. J. *J. Chem. Phys.* **1985**, *82*, 284. (c) Hay, P. J.; Wadt, W. R. *J. Chem. Phys.* **1985**, *82*, 299.

(12) Cotton, F. A.; Feng, X. *J. Am. Chem. Soc.* **1997**, *119*, 7514.

(13) Wierzbicki, A.; Salter, E. A.; Hoffman, N. W.; Stevens, E. D.; Van Do, L.; VanLoock, M. S.; Madura, J. D. *J. Phys. Chem.* **1996**, *100*, 11250.

(14) Gaussian 94, Revision D.3; Frisch, M. J.; Trucks, G. W.; Schlegel, H. B.; Gill, P. M. W.; Johnson, B. G.; Robb, M. A.; Cheeseman, J. R.; Keith, T.; Petersson, G. A.; Montgomery, J. A.; Raghavachari, K.; Al-Laham, M. A.; Zakrzewski, V. G.; Ortiz, J. V.; Foresman, J. B.; Cioslowski, J.; Stefanov, B. B.; Nanayakkara, A.; Challacombe, M.; Peng, C. Y.; Ayala, P. Y.; Chen, W.; Wong, M. W.; Andres, J. L.; Replogle, E. S.; Gomperts, R.; Martin, R. L.; Fox, D. J.; Binkley, J. S.; Defrees, D. J.; Baker, J.; Stewart, J. P.; Head-Gordon, M.; Gonzalez, C.; Pople, J. A. Gaussian Inc.: Pittsburgh, PA, 1995.

(15) Dunning Jr; T. H.; Hay, P. J. In *Modern Theoretical Chemistry*; Schaefer III, H. F., Ed.; Plenum: New York, 1976; p 1.

(16) teXsan: Structure Analysis Software, Molecular Structure Corp: The Woodlands, TX.

(17) Walker, N.; Stuart, D. *Acta Crystallogr. Sect. A* **1983**, *39*, 158.

(18) Beurskens, P. T.; Admiraal, G.; Beurskens, G.; Bosman, W. P.; Garcia-Granda, S.; Smits, J. M. M.; Smykalla, C. The DIRDIF program system; Technical Report of the Crystallography Laboratory, University of Nijmegen, The Netherlands, 1992.

(19) Burla, M. C.; Camalli, M.; Cascarano, G.; Giacovazzo, C.; Polidori, G.; Spagna, R.; Viterbo, D. *J. Appl. Crystallogr.* **1989**, *22*, 389.

(20) Sheldrick, G. M. SHELXS86, Program for the Automatic Solution of Crystal Structure, University of Göttingen, Germany, 1986.

(21) Johnson, C. K. ORTEP, Report ORNL-5138, Oak Ridge National Laboratory, TN, 1976.

(22) Basu Baul, T. S.; Tiekink, E. R. T. *Main Group Met. Chem.* **1993**, *16*, 201.

(23) Beagley, B.; McAloon, K.; Freeman, J. M. *Acta Crystallogr. Sect. B* **1974**, *30*, 444.

(24) Lefferts, J. L.; Molloy, K. C.; Hossain, M. B.; van der Helm, D.; Zuckerman, J. J. *J. Organomet. Chem.* **1982**, *240*, 349.

(25) Frank, W.; Reiss, G. J.; Kuhn, D. *Acta Crystallogr. Sect. C* **1994**, *50*, 1904.

(26) (a) Lindley, P. F.; Carr, P. *J. Cryst. Mol. Struct.* **1974**, *4*, 173. (b) Alcock, N. W.; Culver, J.; Roe, S. M. *J. Chem. Soc., Dalton Trans.* **1992**, 1477.

(27) Hook, J. M.; Linahan, B. M.; Taylor, R. L.; Tiekink, E. R. T.; van Gorkom, L.; Webster, L. K. *Main Group Met. Chem.* **1994**, *17*, 293.

(28) Glusker, J. P.; Lewis, M.; Rossi, M. In *Crystal Structure Analysis for Chemists and Biologists*; VCH: New York, 1994.